

How waves are accelerating global coastal overtopping

Rafael Almar^{1,*}, Harold Diaz¹, Erwin W.J. Bergsma¹, Roshanka Ranasinghe^{2,3,4}, Angelique Melet⁵,
Fabrice Papa¹, Michalis Vousdoukas⁶, Panagiotis Athanasiou^{3,4}, Olusegun Dada⁷, Luis Pedro
Almeida⁸, and Elodie Kestenare¹

¹LEGOS (CNRS/IRD/CNES/Toulouse University), Toulouse, France

²Department of Coastal and Urban Risk @ Resilience, IHE Delft Institute for Water Education, P.O. Box 3015 2610 DA
Delft, The Netherlands

³Harbour. Coastal and Offshore Engineering, Deltares, PO Box 177, 2600 MH Delft, The Netherlands

⁴Water Engineering and Management, Faculty of Engineering Technology, University of Twente, PO Box 217, 7500 AE
Enschede, The Netherlands.

⁵Mercator-Ocean, Toulouse, France

⁶European Commission, Joint Research Centre (JRC), Ispra, Italy

⁷Federal University of Technology, Akure, Nigeria

⁸Universidade Federal do Rio Grande do Sul, Rio Grande, Brazil

Corresponding author *rafael.almar@ird.fr

ABSTRACT

The world's coastal areas are home to about 10% of the human population and support unique and dynamic ecosystems, offering € trillions worth of environmental and societal benefits. Climate change and anthropogenic pressures are however exacerbating devastating hazards such as episodic coastal flooding, the magnitudes of which remain highly uncertain to date. This study, for the first time, presents global scale coastal overtopping estimates, which account for not only the effects of sea level rise, storm surge and wave setup as traditionally done, but also that of wave runup and existing coastal protection measures. While the latter are widely recognized as important determinants of episodic coastal flooding, they have hitherto been ignored in assessments thereof. Our results show that the combination of tides and large wave runup events is the main contributor to episodic coastal overtopping. The Gulf of Mexico, northern Europe, Mediterranean region, east coast of Africa, south east Asia, and north western Australia emerge as hotspots of episodic coastal overtopping under the current climate. Future projections of overtopping with the the global mean sea level rise under "business-as-usual" scenario RCP 8.5 indicate that the globally integrated number of annual overtopping hours will increase at a rate faster than that of the global mean sea level rise itself. This study also shows that, under the RCP 8.5 sea level rise trajectory, the projected acceleration in coastal overtopping should be starting about now and will be clearly discernible by about 2050. Global overtopping has increased almost by 1.5 from 1993 by now and will reach values more than 50 times larger by the end of the 21st century. The global projections presented here are anticipated to lay a solid foundation for the development of effective climate adaptation measures at the identified hotspots, ideally through detailed local scale studies.

33 **Context**

34 Coastal flooding is threatening human societies (Hinkel et al., 2014; Vousdoukas et al., 2018) and infrastructures (Koks et
35 al., 2019) and sea level rise is expected to exacerbate the situation in the decades to come. Over the next few decades, sea
36 level rise is projected to double the frequency of coastal flooding (Vitousek et al., 2017) possibly affecting an estimated
37 global population of nearly 1 billion people (Nicholls and Small, 2002; Neumann et al., 2015; Kulp et al., 2019). Regions
38 with limited water-level variability, i.e., short tailed flood-level distributions, that are located mainly in the Tropics, are
39 likely to be the most affected (Vitousek et al., 2017). In particular, the low-lying coasts of Africa and Asia are thought to be
40 the most vulnerable areas worldwide, at which an increase in flood occurrence could force population migration (Nicholls
41 and Cazenave, 2010). Without appropriate flood mitigation strategies, sea level rise will increase the frequency and
42 magnitude of flooding events (Tebaldi et al., 2012; Vitousek et al., 2017; IPCC report, 2018).

43 Total water level (EWL) at the coast results from several contributions (**Figure 1**). The main contributors differ
44 according to time scales and region; they include contributions by regional sea level ocean governed by the steric effect
45 and circulation (here referred as *SLA*), storm surge due to atmospheric pressure and winds (*DAC*), astronomical tide (*AT*)
46 and wave effects here named runup (*R*) including a time-averaged component (setup) and an oscillatory component
47 (swash) (see Melet et al., 2018).

48

$$49 \quad \text{TWL} = \text{SLA} + \text{DAC} + \text{AT} + R \quad (1)$$

50 Despite the important role that ocean waves play in determining total water level at the coast (Beetham and Kench,
51 2018; Melet et al., 2018) via wave setup and wave runup, their contribution is still largely ignored or underestimated in
52 most studies, mainly due to the lack of global information on detailed coastal topography, knowledge of which is required
53 to compute the wave contributions accurately. Topographic and foreshore slope data available till now, excepting for small
54 local data sets acquired for site specific studies, are often very coarse, outdated or simply non-existent in large parts of the
55 world, leading to inaccurate estimates of flooding and associated risks to coastal populations. Owing to this, global studies
56 (Vitousek et al., 2017; Beck et al., 2018; Melet et al., 2018; Vousdoukas et al., 2018) that do account for the contribution of
57 waves to sea level at the coast are still based on highly simplified coastal topography/bathymetry (e.g. constant slope
58 worldwide). While many studies have acknowledged that local topography and foreshore slope can influence flood
59 exposure and risk greatly (Vousdoukas et al., 2018; Luijendijk et al., 2018; Hauer et al., 2020; Minderhoud, 2019; Kulp et
60 al., 2019), no concerted efforts have been taken to address this shortcoming to date.

61 In this study, we overcome this long-felt need by combining a new state-of-the-art global digital surface model (ALOS
62 World 3D - 30m AW3D30, JAXA – Tadono et al., 2016; Zhang et al., 2019) with water level variations at the coast derived
63 from a combination of satellite altimetry, tide and surge models and wave reanalyses, including the important contribution
64 of wave runup. Using these data, we present, for the first time, global scale estimates of the acceleration of overtopping in
65 recent decades and under one high-end sea level rise scenario.



66

67 **Figure 1.** Schematic of process governing coastal overtopping and different levels of consequent flooding depending on
 68 type of coastal topography. Total water level at the coast results from several contributions: regional sea level governed by
 69 the steric effect and circulation (here referred as *SLA*), astronomical tide (*AT*), surge due to atmospheric pressure and
 70 winds (*DAC*) and wave runup (*R*), decomposed into a time-averaged component (setup) and an oscillatory component
 71 (swash) (see Melet et al., 2018).

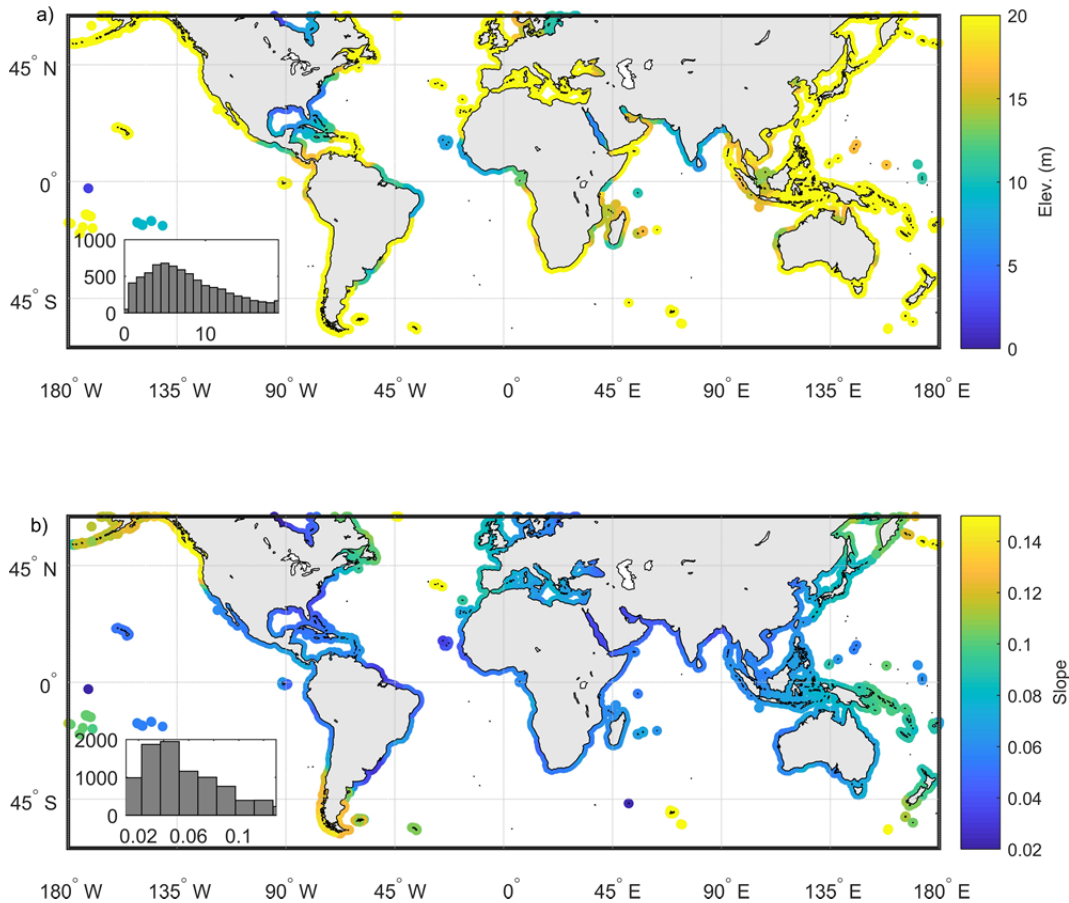
72 **World coastal morphology**

73 The length of the global coastline exceeds 1.6 million kilometers (Burke et al., 2001) including open coasts, bays, lagoons
 74 and estuaries. Among these coastlines, sandy beaches (fine to coarse sand) represent ~31% of ice-free world coasts
 75 (Luijendijk et al., 2018, Vousdoukas et al., 2020). In general, sandy beach slopes range from 0.01 (for finer sediment) and
 76 0.2 (for gravel beaches) (Poate et al., 2016). For these sandy beaches, as a rule of thumb, the wave setup is 20% of offshore
 77 wave height (Stockdon et al., 2006; Dodet et al., 2019). At rocky coasts with rocky platforms, wave runup is important but
 78 reduced by bottom friction over the rocky bottom (Dodet et al., 2018).

79 Coastal morphology has been modified in various ways by human activities, particularly in urbanized areas in which,
 80 for example ports have been constructed, seawalls built to combat coastline recession, cliffs stabilized, and groins placed
 81 in an attempt to retain a beach fringe and maintain dunes (Serafin et al., 2019). These human interventions to the natural
 82 system generally have steepened coastal slopes (e.g. seawalls, dikes), resulting in smaller wave dissipation zones
 83 compared to natural coasts. Variations in sediment budgets, due to, for example, fluvial sediment retention by dams
 84 (Anthony et al., 2015; Latrubesse et al., 2017; Besset et al., 2019; Ranasinghe et al., 2020), urbanization and certain land
 85 use practices (agriculture, deforestation of mangroves; see Luijendijk et al., 2018; Mentaschi et al., 2018), have also made
 86 coastal zones highly vulnerable to overtopping and consequent flooding (MacGranahan et al., 2007; Adelekan, 2010;
 87 Appeaning Addo et al., 2011).

88 **Figure 2** shows the global distribution of the key coastal topographical parameters used in this study (see Data and
 89 Methods for the steps followed to obtain these parameters). The coastal elevations shown in Figure 2(a) are the maximum
 90 subaerial coastal elevations (including dunes and coastal structures). The global average value of the subaerial beach slope

91 is ~ 0.1 (median ~ 0.04), covering different types of coastlines (**Figure 1**) including open sandy beaches, barrier islands,
92 cliffs, river deltas, and engineered beaches (Schwartz, 2003). Regional patterns are clearly visible, such as the along-coast
93 gradient in beach slope along the west coast of North America, from relatively low (0.04) in the tropics to steep (0.15) in
94 high latitudes. Similar features are observed in the southern hemisphere. Africa, the continent with the largest length of
95 sandy coasts, generally has low-lying coastlines with gentle slopes. Interestingly, coastal elevation (see computation
96 method in the Data and Methods Section) appears to generally increase with latitude, while island archipelagos such as
97 Indonesia and Japan show high variability of slope/elevation within small distances (**Figure 2**).
98



99
100 **Figure 2.** Global coastal topography along the world coasts. a) Maximum subaerial coastal elevation and b) subaerial beach
101 slope. Inserts show the distribution of elevations (median=7m) and coastal slopes (median=0.04).

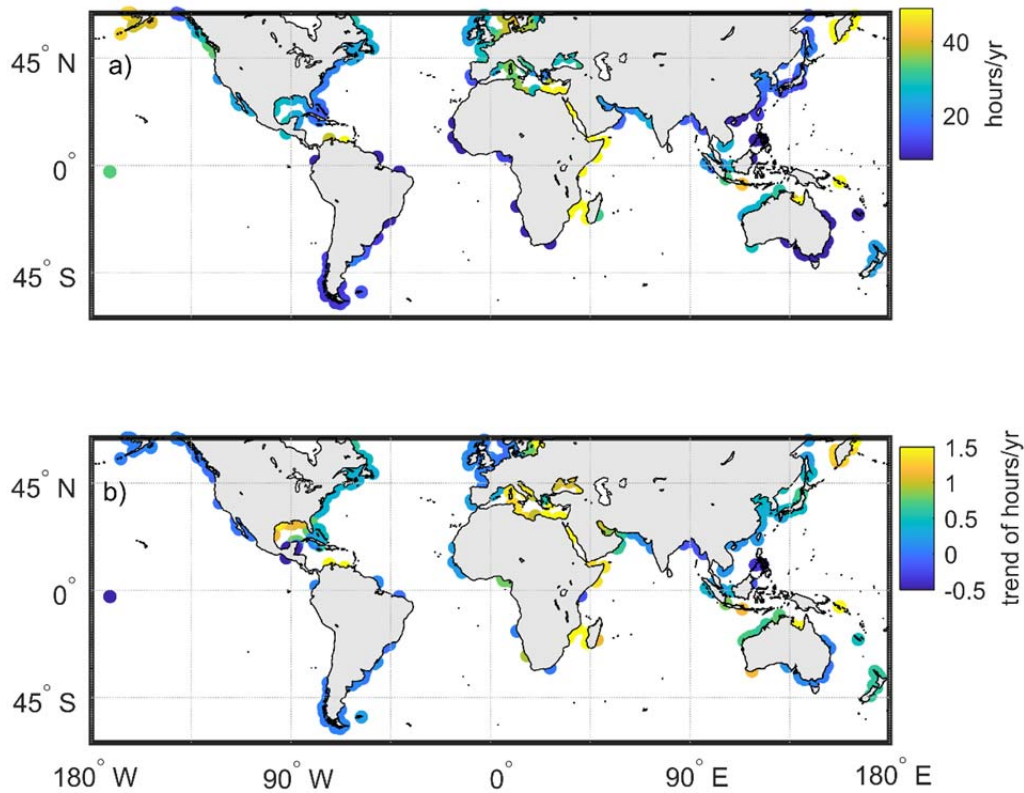
102 Overtopping events

103 Overtopping occurs when the coastal water level exceeds that of the crest level of natural (e.g. dunes) or artificial (e.g.
104 dykes) coastal defenses. Here we used Eq. 1 to compute total water levels over the 23-year period between 1993 and
105 2015. The way in which each term in Eq. 1 is described in detail in the Data and Methods section. Nevertheless, for the
106 convenience of the reader, here a very brief description is given.

107 In all, **Eq. 1** was applied at 14,140 coastal profiles around the world. Regional sea level (SLA) at each computational profile
108 was derived from satellite altimetry sea level time series from the SSALTO/DUACS multimission data (Pujol et al., 2016).
109 Storm surge values (DAC) for the study period were taken from a global application of the MOG2D-G model (Carrere et al.,
110 2014), forced with ERA-interim winds and surface atmospheric pressure. Astronomical tides (AT) were taken from the
111 global tide model FES (Carrere et al., 2014). Wave runup (R, which here includes both wave setup and the oscillatory swash
112 component) was computed using two forms (for steep and mild slopes) of the commonly used Stockdon et al. (2006)
113 parameterization together with ERA-interim wave data.

114 **Figure 3.a** shows the estimated total annual overtopping hours, averaged over 23 years (1993-2015), noting that these
115 results do not account for small-scale coastal defences that are not resolved by the satellite-based AW3D30 data set. A
116 few exposed low-lying regional hot-spots are evident in South East Asia, Northern Europe, Southern Mediterranean coast,
117 and Eastern-US. Among these, the low-lying sedimentary plains such as deltas (e.g. Bengal, Nile and Mississippi Deltas for
118 instance, see Nicholls et al., 2007 and Besset et al., 2019) emerge as the areas in the world that are most threatened by
119 episodic coastal flooding. A detailed validation of our methodology for selected historical events (e.g. Katrina in USA,
120 Xynthia in Europe/France) is provided in Supplementary Material **Section 3**.

121 **Figure 3.b** shows that, over the period 1993-2015 there has been an increasing trend in the total annual overtopping hours
122 in most parts of the world. A few areas appear to have experienced a small trend, mainly in the mid to high latitudes: West
123 coast of North America, North Europe, and the South East coast of South America. The increasing trends are mainly in the
124 tropics, as also observed by Vitousek et al. (2017) and Vousdoukas et al. (2018); e.g. The Gulf of Mexico, northern Europe,
125 Mediterranean region, east coast of Africa, south east Asia, and north western Australia. This might be explained by the
126 fact that in some of these regions generally have little variability in total water level (variance of the time series), and
127 hence, even small increases in sea level (regional relative sea level rise) have a bigger impact on overtopping (Rueda et al.,
128 2017). In the Pacific Basin, the increasing trend on the Western side and a decreasing trend on the Eastern side is
129 noteworthy, as is the strong increasing trend in the Western Indian Ocean along Madagascar and Africa coastlines such as
130 Mozambique. Similar behaviour is also observed in the North Atlantic with a decreasing trend on the Western side and an
131 increasing trend on the Eastern side. Supplementary **Figure S2** shows the trends in wave runup, regional sea level and
132 atmospheric tide separately, indicating that the individual components have contrasting regional patterns. In some areas
133 (e.g. Caribbean, Bay of Bengal, Mekong delta) the contribution of all individual components add up to result in a higher
134 overall trend of overtopping events, whereas in other areas (e.g. North Western Europe, southeastern coast of North
135 America), some components cancel out the effect of others to result in small or negative trends in overtopping events.



136

137 **Figure 3.** Global map of coastal overtopping (number of hours per year): a) occurrence and b) 23 year trend of occurrences
 138 (see methods for details on computation approach adopted).

139

140

141

142

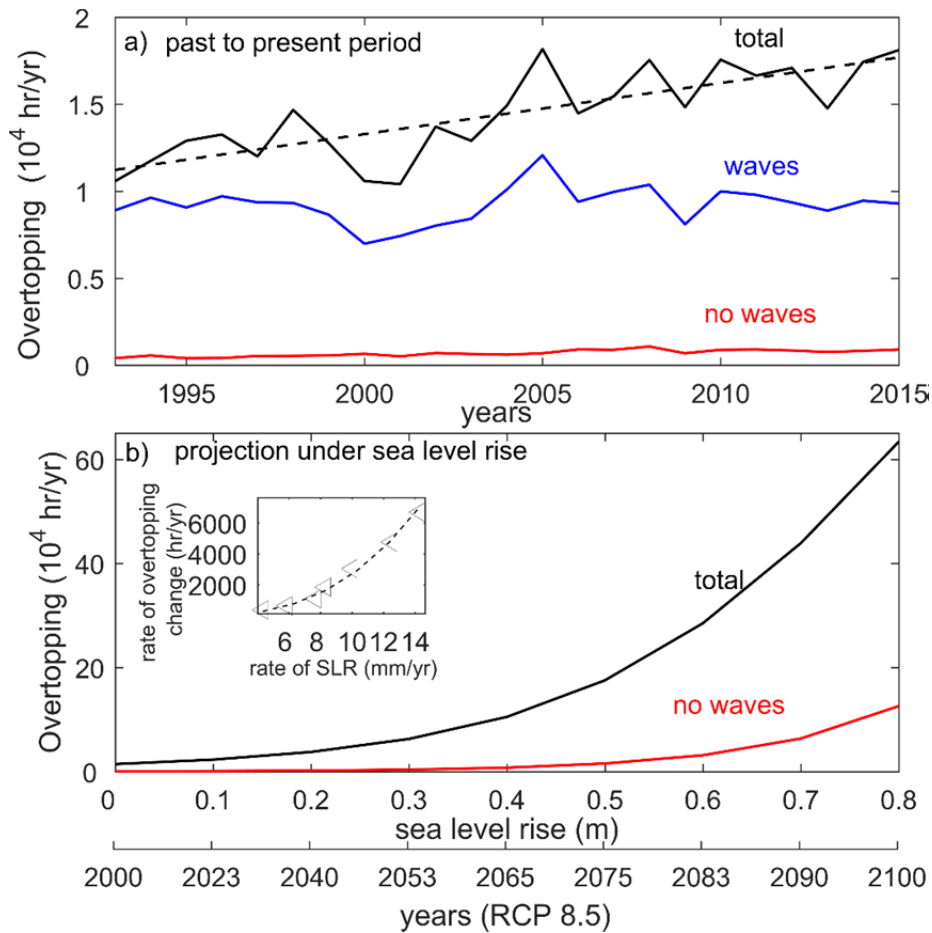
143

144

145

146

Figure 4 shows the globally integrated number of annual overtopping hours (black), the contribution to overtopping from wave runup and tide (not including regional sea level and surge) (blue), and the contribution to overtopping from regional sea level, surge and tide (no waves) (red). **Figure 4a** indicates that wave runup+tide is the dominant contributor to the annual number of overtopping hours, although they, on their own, do not induce a positive significant trend in overtopping hours (the absence of current global trend in waves is also mentioned in Melet et al., 2018). It is the combination of all the components that induces an increase (significant at 95% level using Mann-Kendall test) of the globally integrated number of annual overtopping hours over the past 23 years. Global overtopping has increased almost by 1.5 from 1993.



147

148 **Figure 4.** a) Globally integrated number of annual overtopping hours (solid black line) together with its linear regression
 149 (dashed line) (significant at 95% level), contribution to overtopping from waves and tide only (solid blue line), and the
 150 contribution to overtopping excluding waves (solid red line). b) Globally integrated number of annual overtopping hours
 151 (solid black line) and annual overtopping hours when the wave contribution is excluded (solid red line) under the global
 152 mean sea level rise projected for the Representative Concentration Pathways (“business-as-usual”) RCP 8.5 (median
 153 projection, IPCC AR5 WGI SPM). Insert in b) compares the rates of changes of sea level rise (in mm/yr) with the rate of
 154 overtopping (in hours/yr). Triangles are computed values and dashed line is the fitted exponential regression ($R^2=0.8$)
 155 evidencing a law in $\exp(2.7)$ between the two.

156 The way in which sea level rise may influence the above presented current climate coastal overtopping characteristics was
 157 investigating by computing the change in the annual overtopping hours between year 2000 and 2100, under the median
 158 sea level rise projection for the Representative Concentration Pathways (“business-as-usual”) RCP 8.5 (IPCC AR5 WGI SPM).
 159 **Figure 4.b** shows that, in a globally aggregated sense, if wave runup were not to be considered in computations, the total
 160 annual overtopping hours by 2100 would be underestimated by over 40%. **Figure 4.b** also shows that, when the wave
 161 contribution is included in the computation, a noticeable sea level rise driven increase in overtopping hours is estimated to
 162 have already started (in around 2020), as indicated by the upward inflection in the black line around 2020, while without
 163 wave contributions, a noticeable increase in overtopping hours is only expected to commence around 2075. These future

164 projections indicate that the inevitable sea level rise driven increase of global overtopping will be accelerated by the effect
165 of wave runup, with values more than 50 times larger by the end of the 21st century than for the present period.

166

167 **Discussion and looking forward**

168 Here, we combine fine-scale global coastal topography from recently developed global satellite-based products with state-
169 of-the-art computations of total water level at the coast (including wave contributions) to quantify overtopping exposure
170 worldwide, both for the present and the future. We demonstrate that overtopping events are in fact mainly due to the
171 combined effect of large wave runup events and high astronomical tides. However, these contributing processes by
172 themselves do not induce a significant trend in the globally integrated number of annual overtopping hours, rather, it is
173 the combination of regional sea level, wave runup and tide that results in an increase of this quantity. Thus, our results re-
174 affirm the previously reported (Prime et al., 2016; Serafin et al., 2017) finding that sea-level rise will have a greater impact
175 on 21st century coastal flooding than future changes in wave climate). The interaction of sea level and topography
176 increases overtopping events at a rate faster than sea level rise itself with a found exponential factor of 2.7 with SLR.
177 Under the RCP 8.5 sea level rise trajectory, the projected acceleration in coastal overtopping should be starting about now
178 and will be clearly discernible by about 2050.

179 It should be noted that waves have a significantly different impact on open coasts than on deltas. Recent studies have
180 shown that waves might have a complex influence on flooding at inlets and estuaries, in combination with local hydrology
181 and other sea level contributions deriving from met-ocean forcing (Tazkia et al., 2017; Lashley et al., 2019), but these
182 processes could not be accounted for in our global scale study. Moreover, local precipitation or river discharge can lead to
183 compound flood events when they occur concurrently with storm surge and large wave runup events (Brammer, 2014;
184 Ward et al., 2018; Moftakhari et al. 2017; Paprotny et al., 2020). Again due to the the global focus of this study, such
185 compound flooding events, which are heavily dependent on local phenomena, could not be taken into account in this
186 study.

187 Global scale coastal flooding studies currently face a double observational bottleneck. On one hand, it is currently
188 impossible to observe sea levels at the coast, in particular wave contributions. On the other hand, accurate measurements
189 of regional morphological evolution (Serafin et al., 2019; Mentaschi et al., 2018) and subsidence trends (Becker et al.,
190 2018) also cannot be currently obtained from ground-based GPS stations and satellite surface tracking (altimeter or stereo
191 imagery). Of these, at least the former challenge will however be addressed to some degree by the NASA/CNES altimetry
192 mission Surface Water and Ocean Topography (SWOT), planned for 2021). This mission is expected to accurately monitor
193 water levels in the coastal zone at high resolution (< 100 m, see Durand et al., 2010). The recently launched NASA mission
194 IceSat-2, with its 90-day global revisit and fine resolution (0.7 m along track, 70 m cross track, 30x30 m final products) will
195 also help address this challenge.

196 The global scale of the analysis presented here imposes some further inevitable simplifications in the wave runup
197 calculation; accurate modelling of flooding during storm surges has been conducted at regional scale (Krien et al., 2017;
198 Vousedoukas et al., 2018) but modelling wave propagation to nearshore is a challenge in itself, primarily because coastal

199 bathymetry is generally outdated or unknown at most of the coastlines. Even if detailed present day bathymetry were
200 available, past and future bathymetry would still remain unknown. As a result, this and other recent global studies, use a
201 fixed coastal bathymetry over time periods spanning 50 – 100 years. However, coastal systems are among the most
202 dynamic geological environments on Earth at various time scales, with, for e.g a single large storm being able to reshape
203 regional bathymetry which could significantly affect instantaneous total water levels at the coast in subsequent years.
204 Thus the consideration of passive coastal bathymetry over a 100 years in this and other global studies necessarily assumes
205 that computed coastal flooding is an exclusive response to water levels (Le Cozannet et al., 2019; Serafin et al., 2019).

206 Finally, here we have used only global mean sea level rise projections in our future overtopping computations.
207 However, regional variations in sea level can be significant (Church et al., 2013; Slangen et al., 2014), while local
208 phenomena such as vertical land movement (e.g. land subsidence) can in places result in relative sea level rise rates that
209 are far greater than the global mean rate (e.g. Jakarta, New Orleans, Ho Chi Minh City) (Nicholls et al., 2014). Consideration
210 of these regional and local contributions to relative sea level rise will affect coastal flooding projections for certain specific
211 locations, in particular at coastal cities and low lying deltas (Hallegatte et al., 2013; Erkens et al., 2015 Brown and Nicholls,
212 2015; Kulp and Strauss, 2019; Becker et al., 2020).

213

214 **Data and Methods**

215 **AW3D30 Global Digital Surface Model**

216 Here we used the new and freely available ALOS Global Digital Surface Model (ALOS World 3D - 30m, JAXA - Tadono et al.,
217 2016; Zhang et al., 2019), known as AW3D30. This database is used here with its maximum freely available resolution of 1
218 arc-second (i.e. approximately 30 m, while commercial AW3D PRISM resolution is 5 m). The surface model was acquired
219 over the 2006-2011 period using optical stereo-based photogrammetry and has been made publicly available at 30 m
220 resolution. The AW3D30 product is created as a digital surface model converted from the GRS80 ellipsoid height based on
221 the ITRF97 coordinate system, using the EGM96 geoid model. Our analysis is restricted to the coverage of AW3D30, from
222 60 degrees north to 60 degrees south. High latitudes associated with no-data or low-quality area are discarded in this
223 analysis.

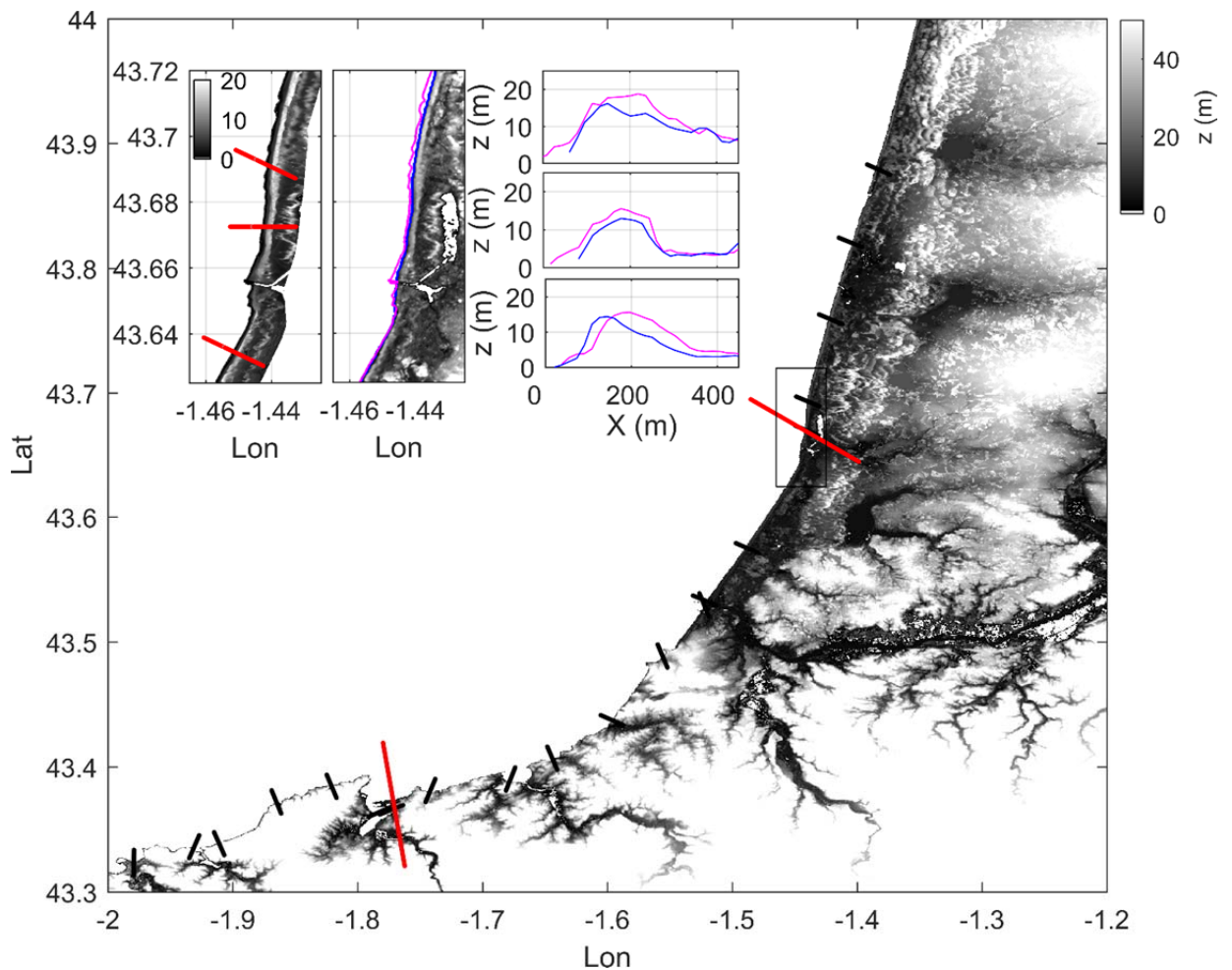
224 A comparison of results obtained using AW3D30 against those obtained using a different independent dataset, from
225 the MERIT and GEBCO topo-bathymetry dataset (Athanasidou et al., 2019) is presented in the Supplementary Material
226 **Section 2**. This latter dataset was used in the study to obtain foreshore slopes that are required as input for the wave
227 runup formulae. To account for artificial coastal protection, the FLOOD PROtection Standards FLOPROS (Scussolini et al.,
228 2016) dataset was used as a third estimate of maximum subaerial coastal elevations (Vousdoukas et al., 2018).

229 **Coastal topography extraction**

230 Maximum subaerial coastal elevation and coastal slopes were extracted from the above-mentioned MERIT and AW3D30
231 dataset along the global coastline. Here, the Global Self-consistent, Hierarchical, High-resolution Geography Database
232 (GSHHS - Wessel and Smith, 1996) coastline "h" highest resolution (~kilometric) was used. Coastal shoreline and
233 topography are highly variable alongshore. In order to obtain reasonably robust estimates, cross-shore aerial topography

234 profiles were extracted every 0.05 degrees (see **Figure 5**). From these, a “median profile” was calculated every 0.5 degrees
235 to construct the profiles ultimately used in the analysis to bring down the computational demands to a manageable level.
236 Islands with a circumference less than 0.5 degrees were excluded from the analysis, as we deemed it sufficient at a global
237 scale and representative of the regional values seen in the literature. This results in a total of 14140 profiles at which the
238 analysis was performed.

239 The topographic slope and maximum elevation on each analysis profile were calculated using an automated detection
240 method. In this method, first, the local sea-land orientation of each profile was identified, based on the average
241 topography values on the two sides of the shoreline: the higher side is taken to be land and lower to be sea. On each
242 transect, the highest coastal point (e.g. dune, cliff top, crest of structure) was approximated as the closest local maximum
243 landward of the determined shoreline (see **Figure 5**). The slope used in the wave contribution calculations is estimated as
244 the average slope within the region determined by the shoreline and the distance given by the coast high, following the
245 method developed in Diaz et al. (2019) – see insert in **Figure 5**.



246

247 **Figure 5.** Regional AW3D30 topography in SW France compared to airborne LIDAR measurements that serves as reference
248 topography (from Diaz et al., 2019). Black and red represent cross shore profiles examples of fine and coarse resolution,

249 respectively. Insert shows LIDAR and AW3D30 maps and different profiles (red transects). Magenta and blue lines stand for
250 LIDAR and AW3D30 datasets, shoreline and cross-shore transects.

251 **Components of sea level at the coast**

252 Altimetry sea-level timeseries (SLA in **Eq. 1**) are extracted from the gridded daily maps produced by the SSALTO/DUACS
253 multi-mission (Pujol et al., 2016) and distributed by the Copernicus Marine Environment Monitoring Service (Le Traon et
254 al., 2019) using the closest points to the coast therein. Atmospheric variables (surface winds, sea level pressure) and wave
255 data (significant height H_s and peak period T_p) are extracted from the ERA-interim data base, developed by the European
256 Centre for Medium-Range Weather Forecasts model (ECMWF, the WAMDI Group, 1988), at 0.5x0.5 degrees and 6-hr
257 temporal resolution between 1993 and 2015. The ERA-Interim reanalysis uses an ocean wind–wave model coupled to the
258 atmosphere, which has been extensively validated (Sterl and Caires, 2005; Caires et al., 2006; Dee et al., 2011). Surges
259 (named DAC in **Eq. 1**) were extracted from the dynamical atmospheric correction applied to altimetric data, provided by
260 the MOG2D-G barotropic model forced by ERA-interim surface winds and the inverse barometer effect with data outputs
261 at a 6-hourly temporal resolution. Astronomical tide elevations (named AT in **Eq. 1**) were obtained from the global tide
262 model FES (Finite Element Solution – Carrere et al., 2014). Tide predictions were derived with hourly temporal resolution
263 using the closest points to the coast. Wave runup (R in **Eq. 1**) is computed from the conventional and commonly used
264 parameterization by Stockdon et al. (2006), where R is given as a function of deep-water significant wave height H_s , wave
265 length (L_o), and topography slope (β). Here, Stockdon et al.'s (2006) parametrization was used in two forms depending on
266 the ration between the relative coastal slope and incident waves as described by the Iribarren number $\xi =$
267 $\tan(\beta)/(H_s/L_o)$ (Iribarren and Nogales, 1949):

- 268 • **Eq. 2** at coasts with $\xi < 0.3$:

$$269 R = 0.043 \sqrt{H_s L_o} \quad (2)$$

- 270 • **Eq. 3** at coasts with $\xi > 0.3$:

$$271 R = 1.1 (0.35\beta\sqrt{H_s L_o} + 0.5[H_s L_p (0.5625\beta^2 + 0.004)]^{1/2}) \quad (3)$$

272 Stockdon et al.'s (2006) parametrization was developed for and is applicable for sandy beaches. It is however
273 commonly used for different environments, such as gravel beaches (Poate et al., 2016), rocky coasts (Dodet et al., 2018),
274 on structures (Atkinson et al., 2017), with reasonable demonstrated skill in predicting wave runup (Dodet et al., 2019). For
275 example, the automated computation procedures used in this study would ensure that **Eq. 3** would be used at steep profiles
276 such as would be the case where coastal defense structures are present, whereas on natural beaches with milder slopes, **Eq.**
277 **2** would be used.

278

279 **Method to compute overtopping**

280 Using the above described dataset, the different contributions to total water level, including wave runup, were calculated
281 over the 1993-2015 period every hour. Overtopping is defined when the total instantaneous water level thus computed

282 exceeded the maximum coastal elevation, potentially causing flooding. To temporally-aggregate the event level
283 information, the number of hours of water level occurrences exceeding the maximum coastal elevation threshold is
284 counted at each point for every year. The sensitivity of the overtopping projections to the choice of the topography dataset
285 (i.e. AW3D30, MERIT-GEBCO, FLOPROS) was investigated and shown in Supplementary **Figure S5**.

286

287 **Data availability**

288 The SSALTO/DUACS altimeter products were produced and distributed by the Copernicus Marine Environment Monitoring
289 Service (<http://marine.copernicus.eu/>). Dynamical atmospheric corrections were produced by the Collecte Localisation
290 Satellites Space Oceanography Division using the MOG2D model from Laboratoire d'Etudes en Géophysique et
291 Océanographie Spatiales (LEGOS) and distributed by AVISO (Archiving, Validation and Interpretation of Satellite
292 Oceanographic data), with support from Centre National d'Etudes Spatiales (CNES) (<http://www.aviso.altimetry.fr/>).
293 FES2014 tidal data are produced by LEGOS. Tide gauge data were downloaded from the University of Hawaii Sea Level
294 Center (<https://uhslc.soest.hawaii.edu/data>). ERA-Interim data were produced by the European Centre for Medium-Range
295 Weather Forecasts (<https://www.ecmwf.int/en/forecasts/datasets/reanalysis-datasets/era-interim>).

296 **References**

- 297 Adelekan, I. O. Vulnerability of poor urban coastal communities to flooding in lagos, nigeria. *Environ. Urbanization* 22,
298 DOI: [doi:10.1177/0956247810380141](https://doi.org/10.1177/0956247810380141) (2010).
- 299 Anthony, E., Brunier, G., Besset, M. *et al.* Linking rapid erosion of the Mekong River delta to human activities. *Sci Rep* 5,
300 14745 (2015). <https://doi.org/10.1038/srep14745>
- 301 Appeaning Addo, K., Larbi, L., Amisigo, B. & Ofori-Danson, P. K. Impacts of coastal inundation due to climate change in a
302 cluster of urban coastal communities in ghana, west africa. *Remote. Sens.* 3, 2029–2050, DOI: [10.3390/rs3092029](https://doi.org/10.3390/rs3092029)
303 (2011).
- 304 Athanasiou, P., van Dongeren, A., Giardino, A., Vousdoukas, M., Gaytan-Aguilar, S., and Ranasinghe, R.: Global distribution
305 of nearshore slopes with implications for coastal retreat, *Earth Syst. Sci. Data*, 11, 1515–1529,
306 <https://doi.org/10.5194/essd-11-1515-2019>, (2019).
- 307 Atkinson, A. L. *et al.* Assessment of runup predictions by empirical models on non-truncated beaches on the south-east
308 australian coast. *Coast. Eng.* 119, 15 – 31 (2017).
- 309 Beck, M.W., Losada, I.J., Menéndez, P. *et al.* The global flood protection savings provided by coral reefs. *Nat Commun* 9,
310 2186 (2018). <https://doi.org/10.1038/s41467-018-04568-z>
- 311 Becker, M., Karpytchev, M. & Papa, F. Hotspots of relative sea level rise in the tropics. *Trop. Extrem. Nat. Var. Trends*
312 9780128092484 (2018).

313 Becker, M., Papa, F., Karpytchev, M., Delebecque, C., Krien, Y. et al.. Water level changes, subsidence, and sea level rise in
314 the Ganges-Brahmaputra-Meghna delta. Proceedings of the National Academy of Sciences of the United States of
315 America , National Academy of Sciences, 2020, pp.201912921. (10.1073/pnas.1912921117). (hal-02430120)

316 Beetham, E. P. & Kench, P. Predicting wave overtopping thresholds on coral reef-island shorelines with future sea-level
317 rise. *Nat. Commun.* (2018).

318 Besset, M., Anthony, E.J. , Bouchette, F., Multi-decadal variations in delta shorelines and their relationship to river
319 sediment supply: an assessment and review. *Earth Sci. Rev.* (2019), 193-199-219

320 Brammer, H. Bangladesh's dynamic coastal regions and sea-level rise. *Clim. Risk Manag.* 1, 51–62 (2014).

321 Brown, S. & Nicholls, R. Subsidence and human influences in mega deltas: The case of the ganges–brahmaputra–meghna.
322 *Sci. The Total. Environ.* 527-528, 362 – 374 (2015).

323 Burke, L. et al. Pilot analysis of global ecosystems: coastal ecosystems. *World Resour. Institute, Wash. DC* 93 pp (2001).

324 Caires, S., Swail, V. & Wang, X. Projection and analysis of extreme wave climate. *J. Clim.* 19(21), 5581–5605 (2006).

325 Carrere, L., Lyard, F., Cancet, M., Guillot, A. & Picot, N. Fes 2014, a new tidal model – validation results and perspectives for
326 improvements. *Present. to ESA Living Planet Conf. Prague 2016* 137, 553–597 (2014).

327 Church, J. A. et al. Sea-level rise by 2100. *Science* 342, 1445, DOI: [doi:10.1371/journal.pone.0118571](https://doi.org/10.1371/journal.pone.0118571) (2013).

328 Dee, D. & et al. The era-interim reanalysis: configuration and performance of the data assimilation system. *Q. J. R.*
329 *Meteorol. Soc.* 137, 553–597 (2011).

330 Diaz, H., Almar, R. & Bergsma, E. W. J. On the use of satellite-based digital elevation models to determine coastal
331 topography. *IEEE proceedings IGARSS, Jpn.* (2019).

332 Dodet, G. et al. Wave runup over steep rocky cliffs. *J. Geophys. Res. Ocean.* 123(10), 7185–7205, (2018)

333 Dodet, G. et al., 2019. The contribution of wind generated waves to coastal sea level changes. *Surv. Geophys.*

334 Durand, M. et al. The surface water and ocean topography mission: Observing terrestrial surface water and oceanic
335 submesoscale eddies. *Proc. IEEE* 98, 766–779, DOI: [10.1109/JPROC.2010.2043031](https://doi.org/10.1109/JPROC.2010.2043031) (2010).

336 Erkens, G., Bucx, T., Dam, R., de Lange, G. & Lambert, J. Sinking coastal cities. *Proc. IAHS* 372, 189–198 (2015).

337 Hallegatte, S., Green, C., Nicholls, R. & Corfee-Morlot, J. Future flood losses in major coastal cities. *Nat. Clim. Chang.* 3(9),
338 802–806 (2013).

339 Hauer, F. E. M. V. e. a., M.E. Sea-level rise and human migration. *Nat Rev Earth Environ* 1, 28–29 (2020).

340 Hinkel J, Lincke D, Vafeidis AT, Perrette M, Nicholls RJ, Tol RSJ, et al. Coastal flood damage and adaptation costs under 21st
341 century sea-level rise. Proceedings of the National Academy of Sciences; 111: 3292–3297.
342 <https://doi.org/10.1073/pnas.1222469111> pmid:24596428, (2014)

343 IPCC report, 2018, *Special Report on Global Warming of 1.5 °C (SR15)*. <http://www.ipcc.ch/report/sr15/>, IPCC (2018).

344 Iribarren, C., Nogales, C. Protection des ports. XVIIth International Navigation Congress, Section II, Communication, 31–80,
345 (1949)

346 Krien, Y., Dudon, B., Roger, J., Arnaud, G. & Zahibo, N. Assessing storm surge hazard and impact of sea level rise in the
347 lesser antilles case study of martinique. *Nat. Hazards Earth Syst. Sci.* 17, 1559–1571, (2017), DOI: [10.5194/nhess-17-](https://doi.org/10.5194/nhess-17-1559-2017)
348 [1559-2017](https://doi.org/10.5194/nhess-17-1559-2017),

349 Kulp, S. B., Strauss S.A. New elevation data triple estimates of global vulnerability to sea-level rise and coastal flooding. *Nat*
350 *Commun* 10, 4844 (2019).

351 Lashley, C.H.; Bertin, X.; Roelvink, D.; Arnaud, G. Contribution of Infragravity Waves to Run-up and Overwash in the Pertuis
352 Breton Embayment (France). *J. Mar. Sci. Eng.* (2019), 7, 205.

353 Latrubesse, E. M. *et al.* Damming the rivers of the amazon basin. *Nature* 546, 363–369 (2017).

354 Le Cozannet, G. L. *et al.* Quantifying uncertainties of sandy shoreline change projections as sea level rises. *Sci. Reports*
355 9(42)., (2019)

356 Le Traon PY, *et al.*, (2019) From Observation to Information and Users: The Copernicus Marine Service Perspective. *Front.*
357 *Mar. Sci.* 6:234. doi: 10.3389/fmars.2019.00234 Luijendijk, A. *et al.* The state of the world’s beaches. *Sci. Reports* 8,
358 6641 (2018).

359 McGranahan G, Balk D, Anderson B. The rising tide: assessing the risks of climate change and human settlements in low
360 elevation coastal zones. *Environment and Urbanization*, (2007); 19: 17–37

361 Melet, A., Meyssignac, B., Almar, R. & Le Cozannet, G. Under-estimated wave contribution to coastal sea-level rise. *Nat.*
362 *Clim. Chang.* NCLIM–17091712 (2018).

363 Mentaschi, L., Vousdoukas, M., Pekel, J.-F., Voukouvalas, E. & Feyen, L. Global long-term observations of coastal erosion
364 and accretion. *Sci. Reports* 8, 12876 (2018).

365 Minderhoud, C. L. E. G. e. a., P.S.J. Mekong delta much lower than previously assumed in sea-level rise impact
366 assessments. *Nat Commun* 10, 3847 (2019).

367 Moftakhari, H. R., Salvadori, G., AghaKouchak, A., Sanders, B. F. & Matthew, R. A. Compound effects of sea level rise and
368 fluvial flooding. *Proc. Natl Acad. Sci. USA* 114, 9785–9790 (2017).

369 Neumann, B., Vafeidis, A., Zimmermann, J. & Nicholls, R. Future coastal population growth and exposure to sea-level rise
370 and coastal flooding—a global assessment. *PloS one* 10, e0118571, DOI: [doi:10.1371/journal.pone.0118571](https://doi.org/10.1371/journal.pone.0118571) (2015).

371 Nicholls, R. & Cazenave, A. Sea-level rise and its impact on coastal zones. *Science* 328, 1517–1520 (2010).

372 Nicholls, R. *et al.* Coastal systems and low-lying areas: Climate change 2007: impacts, adaptation and vulnerability. *In:*
373 *Parry ML, Canziani OF, Palutikof JP, van der Linden PJ, Hanson CE (eds) Contribution working group II to fourth*
374 *assessment report intergovernmental panel on climate change. Camb. Univ. Press. Cambridge, UK (2007).*

375 Nicholls RJ, Hanson SE, Lowe JA, Warrick RA, Lu X, Long AJ. Sea-level scenarios for evaluating coastal impacts. *Wiley*
376 *Interdisciplinary Reviews: Climate Change*, (2014); 5: 129–150.

377 Paprotny, D., Kreibich, H., Morales-Nápoles, O., Terefenko, P., Schröter, K. Estimating exposure of residential assets to
378 natural hazards in Europe using open data. - *Natural Hazards and Earth System Sciences (NHES)*, 20, 1, 323-343.,
379 (2020)

380 Poate, T. G., McCall, R. T. & Masselink, G. A new parameterisation for runup on gravel beaches. *Coast. Eng.* 117, 176–190
381 (2016).

382 Prime, T., Brown, J. M. & Platera, A. J. Flood inundation uncertainty: The case of a 0.5% annual probability flood event.
383 *Environ. Sci. Policy* 59, 1–9 (2016).

384 Pujol, M.-I. *et al.*, 2014: the new multi-mission altimeter data set reprocessed over 20 years. *Ocean. Sci.* 1067–1090 (2016).

385 Ranasinghe, R. On the need for a new generation of coastal change models for the 21st century. *Sci Rep* 10, 2010 (2020).
386 <https://doi.org/10.1038/s41598-020-58376-x>

387 Rueda, A. *et al.* A global classification of coastal flood hazard climates associated with large-scale oceanographic forcing.
388 *Sci. Reports* 7, 5038 (2017).

389 Schwartz, M. *Encyclopedia of Coastal Science*, Springer, Dordrecht, (2003).

390 Scussolini, P. *et al.* Flopros: an evolving global database of flood protection standards. *Nat. Hazards Earth Syst. Sci.* 16,
391 1049–1061, DOI: 10.5194/nhess-16-1049-2016 (2016).

392 Serafin, K., Ruggiero, P. & Stockdon, H. The relative contribution of waves, tides, and non-tidal residuals to extreme total
393 water levels on us west coast sandy beaches. *Geophys. Res. Lett.* 44, 1839–1847 (2017).

394 Serafin, K. A., Ruggiero, P., Barnard, P. L. & Stockdon, H. F. The influence of shelf bathymetry and beach topography on
395 extreme total water levels: Linking large-scale changes of the wave climate to local coastal hazards. *Coast. Eng.* DOI:
396 <https://doi.org/10.1016/j.coastaleng.2019.03.012> (2019). Slangen *et al.*, (2014)

397 Sterl, A. & Caires, S. Climatology, variability and extrema of ocean waves: the web-based knmi/era-40 wave atlas. *J.*
398 *Climatol.* 25, 963–977 (2005).

399 Stockdon, H. F., Holman, R. A., Howd, P. A. & Sallenger Jr, A. H. Empirical parameterization of setup, swash, and runup.
400 *Coast. Eng.* 53, 573–588 (2006).

401 Tadono, T. *et al.* Generation of the 30 m-mesh global digital surface model by alos prism. *Int. Arch. Photogramm. Remote.*
402 *Sens. Spatial Inf. Sci.* 157–162 (2016).

403 Tazkia A. R., Krien Y., Durand Fabien, Testut Laurent, Islam Akms, Papa Fabrice, Bertin X. Seasonal modulation of M2 tide
404 in the Northern Bay of Bengal. *Continental Shelf Research*, 137, 154-162. ISSN 0278-4343, (2017)

405 Tebaldi, Strauss, Zervas. Modelling sea level rise impacts on storm surges along US coasts. *Environmental Research Letters*
406 7, 12 pp., (2012)

407 Vitousek, S. & *et al.* Doubling of coastal flooding frequency within decades due to sea-level rise. *Sci. Rep.* 7 (2017).

408 Vousdoukas, M., Mentaschi, L., Voukouvalas, E. & Feyen, L. Climatic and socioeconomic controls on coastal flooding
409 impacts in europe. *Nat. Clim. Chang.* 8, 776–780 (2018).

410 Vousdoukas, M.I., Ranasinghe, R., Mentaschi, L. *et al.* Sandy coastlines under threat of erosion. *Nat. Clim. Chang.* 10, 260–
411 263 (2020). <https://doi.org/10.1038/s41558-020-0697-0>

412 Ward, P.J. *et al.*. Dependence between high sea-level and high river discharge increases flood hazard in global deltas and
413 estuaries. *Environ. Res. Lett.* 13 084012, (2018)

414 Wessel, P. & Smith, W. A global, self-consistent, hierarchical, high-resolution shoreline database. *J. Geophys. Res.* 101(B4),
415 8741–8743 (1996).

416 Zhang, K. *et al.* Accuracy assessment of aster, srtm, alos, and tdx dems for hispaniola and implications for mapping
417 vulnerability to coastal flooding. *Remote. Sens. Environ.* 225, 290 – 306, DOI:
418 <https://doi.org/10.1016/j.rse.2019.02.028> (2019).

419

420 **Acknowledgments**

421 RR is supported by the AXA Research fund and the Deltares Strategic Research Programme 'Coastal and Offshore
422 Engineering'

423

1 **Supplementary Material**

2 **How waves are accelerating global coastal overtopping**

3 **Rafael Almar^{1,*}, Harold Diaz¹, Erwin W.J. Bergsma¹, Roshanka Ranasinghe^{2,3,4}, Angelique Melet⁵,**
4 **Fabrice Papa¹, Michalis Voudoukas⁶, Panagiotis Athanasiou^{3,4}, Olusegun Dada⁷, Luis Pedro**
5 **Almeida⁸, and Elodie Kestenare¹**

6 ¹LEGOS (CNRS/IRD/CNES/Toulouse University), Toulouse, France

7 ²Department of Coastal and Urban Risk @ Resilience, IHE Delft Institute for Water Education, P.O. Box 3015 2610 DA
8 Delft, The Netherlands

9 ³Harbour. Coastal and Offshore Engineering, Deltares, PO Box 177, 2600 MH Delft, The Netherlands

10 ⁴Water Engineering and Management, Faculty of Engineering Technology, University of Twente, PO Box 217, 7500 AE
11 Enschede, The Netherlands.

12 ⁵Mercator-Ocean, Toulouse, France

13 ⁶European Commission, Joint Research Centre (JRC), Ispra, Italy

14 ⁷Federal University of Technology, Akure, Nigeria

15 ⁸Universidade Federal do Rio Grande do Sul, Rio Grande, Brazil

16

17 Corresponding author * rafael.almar@ird.fr

18

19

20

21

22

23

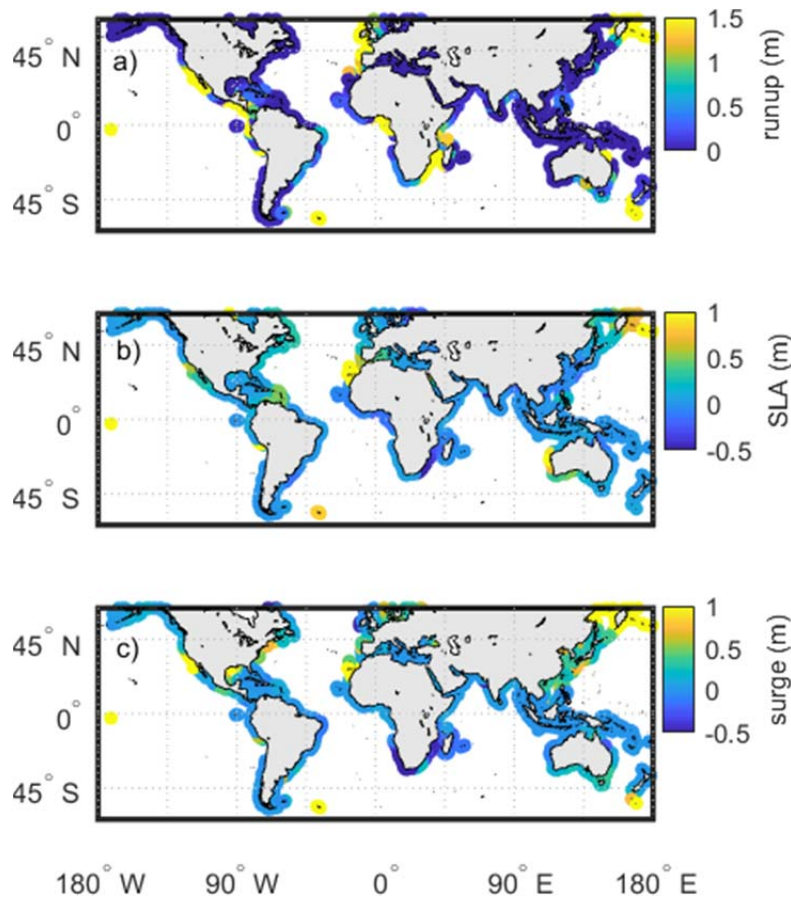
24

25

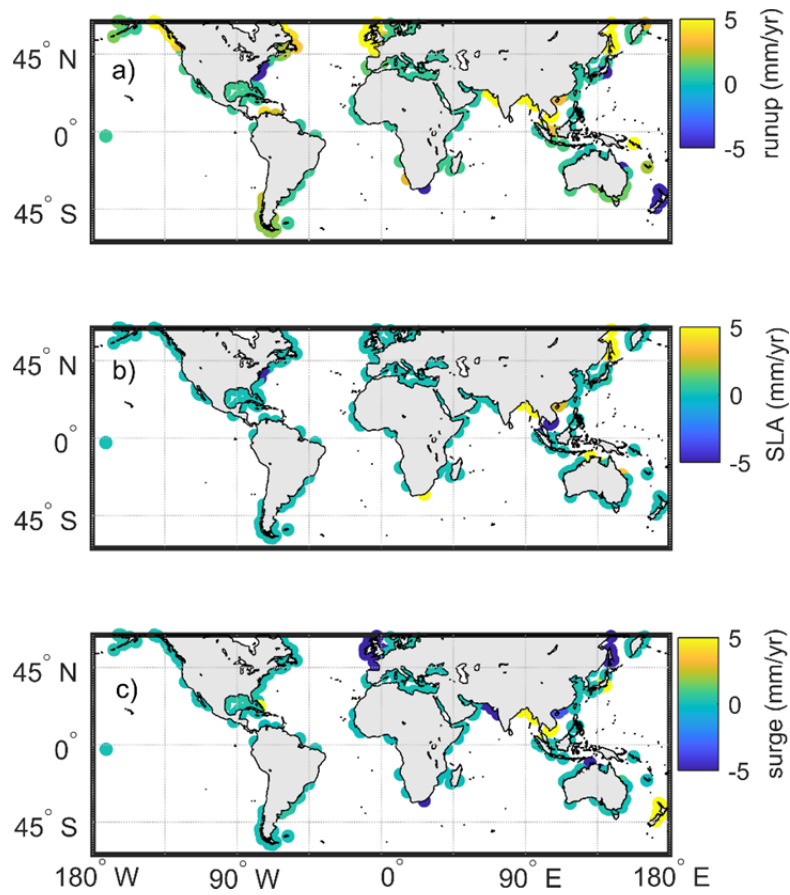
26 **S1. Separation of total water level at the coast trends**

27 **Figure S1** illustrates the decomposition of components wave runoff (R in **Eq. 1**), regional sea level (SLA in **Eq. 1**) and storm
28 surge (DAC in **Eq. 1**, inverse barometer combined with high-frequency barotropic response of the ocean to atmospheric
29 wind and pressure forcing) of sea level at the coast separately (we do not show astronomical tide but it was included in
30 the computation). It is evidenced that the individual components have contrasting regional trend patterns and
31 contributions to overtopping (**Figure 3.a** of the manuscript).

32 **Figure S2** shows the 1993 -2015 trends computed from annual values in wave runoff (R in **Eq. 1**), regional sea level (SLA in
33 **Eq. 1**) and storm surge (DAC in **Eq. 1**) separately, and used to compute the trend in overtppping (**Figure 3.b** of the
34 manuscript). As observed for the average values, the trends have contrasting regional trend patterns. In some areas (e.g.
35 Caribbean, Bay of Bengal, Mekong delta) the contribution of all individual components add up to result in a higher overall
36 trend of overtopping events, whereas in other areas (e.g. North Western Europe, southeastern coast of North America),
37 some components cancel out the effect of others to result in small or negative trends in overtopping events.



38
39 **Figure S1.** Contribution of a) wave runoff (R), b) steric sea level (SLA) and c) storm surge (DAC) to the total overtopping
40 (**Figure 3.a**). Values reflect each average components during the events.



41

42 **Figure S2.** Contribution of a) wave runup (R), b) steric sea level (SLA) and c) storm surge (DAC) to the total overtopping
 43 trend (**Figure 3.b**). These trends are computed from the annual values during the events.

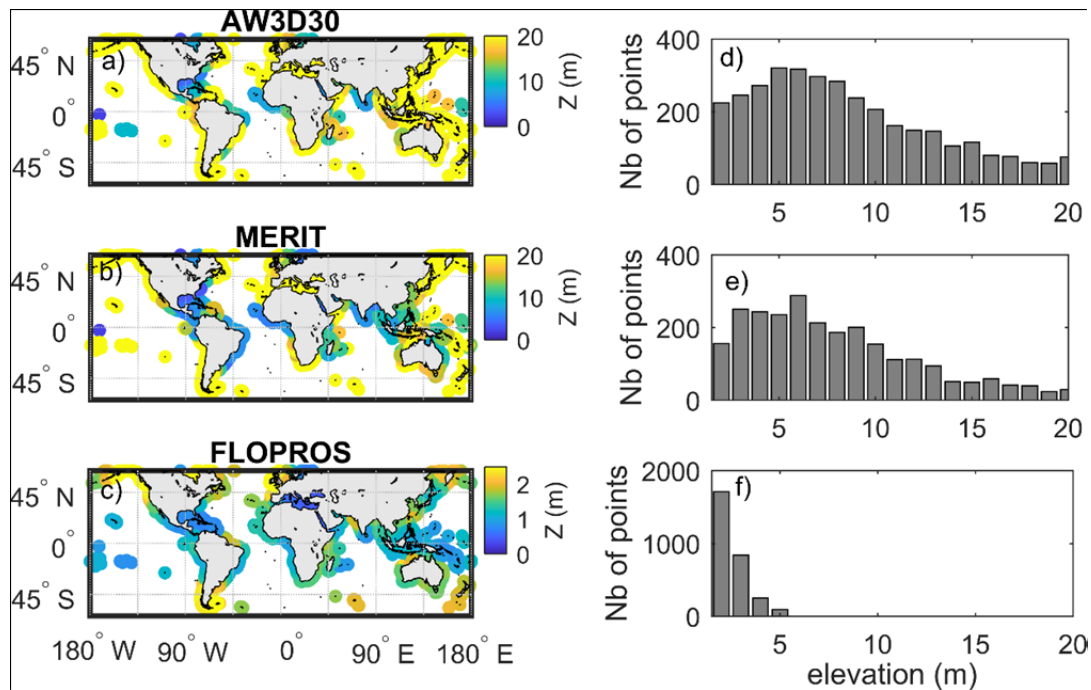
44

45 **S2. Comparison of topography datasets**

46 The way in which the choice of the topography dataset may influence the overtopping results is investigated here. The
 47 capabilities of AW3D30 to derive coastal topography has been investigated in details in Diaz et al. (2019) at Capbreton, SW
 48 France and compared to other satellite-derived topography data sets. These results showed that AW3D30 has good skills
 49 to reproduce the topography of the upper beach (in the latter case), with an overall good estimate of absolute elevation.
 50 AW3D30 was found particularly capable of estimating coastal elevation such as for a dune. The drawbacks are the
 51 limitation in the intertidal area that is generally lacking from the dataset. Her the results obtained using AW3D30 were
 52 compared with different independent datasets, from the MERIT (SRTM) and GEBCO bathymetry dataset (Athanasίου et al.,
 53 2019). This latter dataset was used to obtain a second estimate, in addition to the AW3D30 one, of foreshore slopes that
 54 need to be used in wave runup formulae. To account for artificial coastal protection, the FLOod PROtection Standards
 55 FLOPROS (Scussolini et al., 2016) dataset was used to have a third estimate of coastal elevations and subsequent flooding
 56 (Vousdoukas et al., 2018). These three datasets were used randomly in the projections to reduce the dependence to a
 57 single one in our analyses.

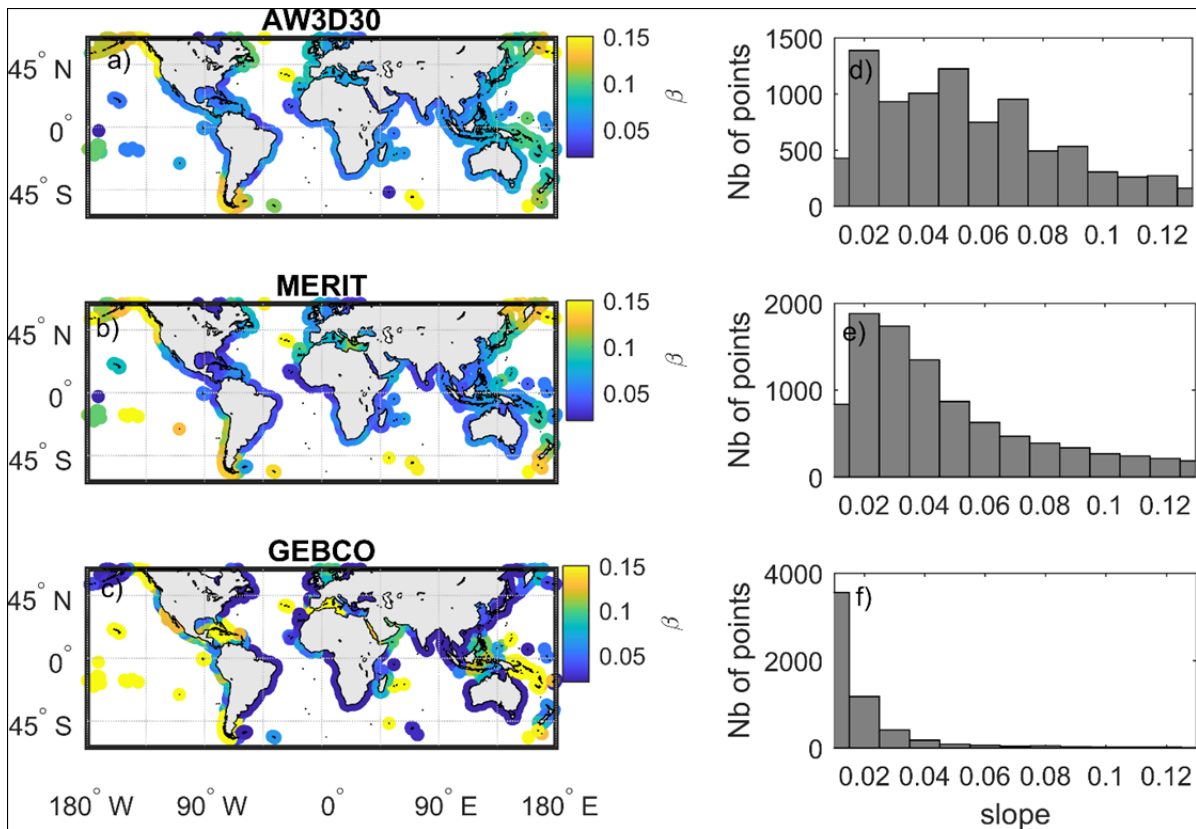
58 The sensitivity of the overtopping projections to the topographic dataset used is investigated here. **Figure S2** indicates that
 59 both FLOPROS and MERIT data bases generally provide lower estimates of maximum subaerial coastal elevation compared
 60 to AW3D-30, which would lead to more flooding when FLOPROS or MERIT is used in the computations (**Figure S4**). **Figure**
 61 **S3** shows that nearshore slopes of GEBCO (slope computed between the depth of closure and the coastline) are milder
 62 when compared with the foreshore slopes of AW3D30 (average slope within the region determined by the shoreline and
 63 the distance given by the coast high), which would to less flooding when using the former. Interestingly, when MERIT and
 64 GEBCO are used for coastal elevation and slope respectively (for runup – see **Figure S3**), projected overtopping appears to
 65 be very close to those obtained when using AW3D30 (**Figure S4**).

66
67

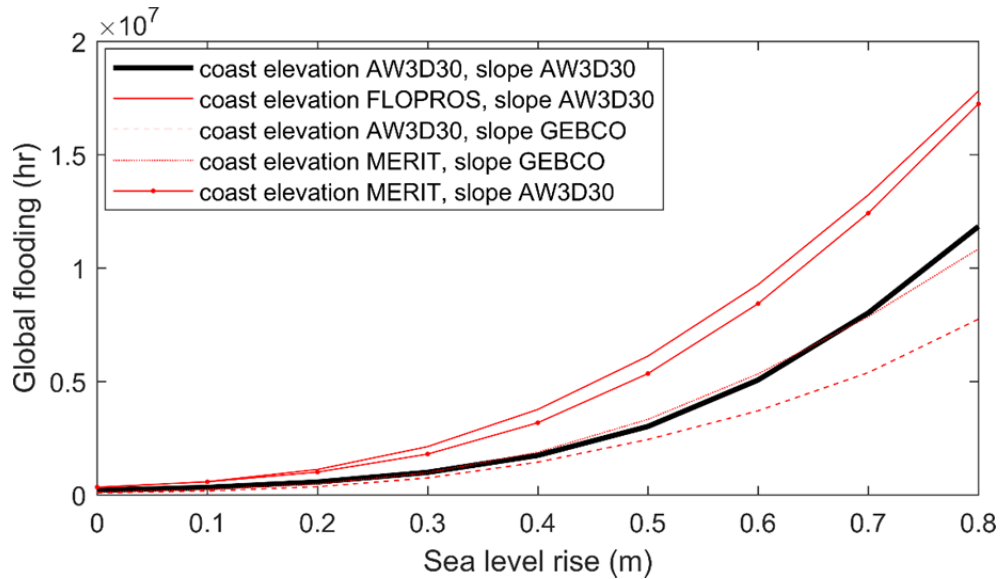


68 **Figure S3.** Global distribution of the maximum subaerial coastal elevation computed from 3 different datasets: AW3D30
 69 (ALOS), MERIT (SRTM), and FLOPROS. Left hand subpanels show worldwide maps. Right hand column bar subpanels show
 70 the distributions.
 71

72



74
 75 **Figure S4.** Global distribution of coastal slopes computed from 3 different datasets: AW3D30 (ALOS), MERIT (SRTM) and
 76 GEBCO. Left panels show the spatial distribution with right panels showing the value distribution. Subaerial highs of
 77 AW3D30 and MERIT are computed vector is the maximum elevation found from the first local maxima, and slopes are
 78 calculated from the shoreline to the maximum elevation point. For GEBCO, the slope is the nearshore slope (from
 79 shoreline till depth of closure) as calculated in Athanassiou et al. (2019).
 80



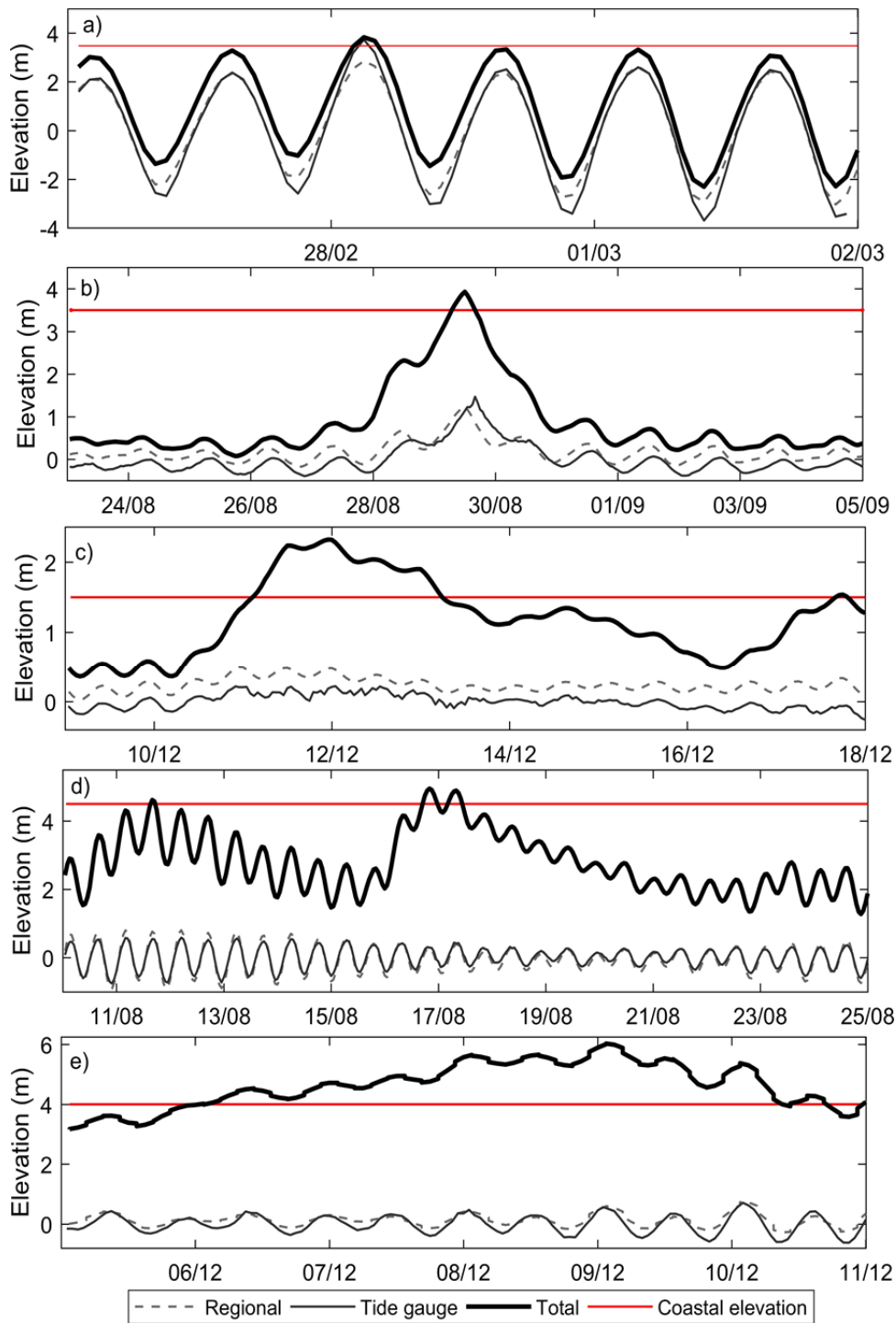
81
 82 **Figure S5.** Sensitivity Globally integrated number of annual overtopping hours to the coastal topography datasets. The
 83 reference dataset used this study for the analyses is ALOS AW3D30 (coastal elevation and slope, thick black line).

84

85 **S3. Validation of the overtopping computations for specific coastal flooding regional events**

86 Here, the methodology adopted to compute overtopping is tested for four documented major events (**Figure S6**) along the
87 West Europe Atlantic coast (**Figure S6.a**, Xynthia storm in France, Bertin et al., 2012), Gulf of Mexico (**Figure S6.b**, Katrina
88 hurricane in USA, Fritz et al., 2007), Mediterranean South-East coast (**Figure S6.c**, Nile delta in Egypt; Frihy et al., 2010;
89 Refaat and Eldeberk, 2016; Ismail, et al., 2012), Gulf of Guinea, West Africa (**Figure S6.d**, Lagos in Nigeria; Nwilo et al.,
90 1997; Olaniyan and Afiesimama, 2003) and Majuro in Marshall Pacific Islands (**Figure S6.e**, Hoeke et al., 2013). The goal is
91 to assess whether our method is able to reproduce the regional sea level at the coast by comparing our calculations with
92 sea level tide-gauge timeseries from the Global Extreme Sea Level Analysis (GESLA) dataset (Woodworth et al., 2017).
93 Finally, the potential of overtopping is investigated by comparing the total sea level at the coast including wave runup.
94 Regional AW3D30 coastal elevations compare well with levels reported in the literature (South West France in Diaz et al.
95 (2019) and around the Iberian Peninsula in Zhang et al., 2018). Our Regional sea levels (TWL minus wave runup) estimate
96 (dashed black) also show a good agreement when compared with GESLA tidal gauges (thin black). It is interesting to
97 observe that regional sea level alone cannot be responsible for overtopping and flooding in these study cases. It is only
98 when wave runup is added that the water level overpasses the coastal elevation maxima for these 4 events. This is evident
99 for the Gulf of Guinea case (**Figure S6.d**) where large tidal (spring) amplitude cannot induce overtopping alone which
100 actually happen with large waves when tide amplitude already reduced. This is particularly the case for Lagos and Pacific
101 Islands events where the flooding is due to distant swell (Hoeke et al., 2013; Ford et al., 2018) by contrast with local storms
102 associated with strong winds and surge (i.e. Xynthia and Katrina).

103



104

105 **Figure S6.** Validation of event detection with reported flooding through overtopping: a) along the West Europe Atlantic
 106 coast (Xynthia storm in France, Bertin et al., 2012), b) Gulf of Mexico (Katrina hurricane in USA, Fritz et al., 2007), c)
 107 Mediterranean South-East coast (Nile delta in Egypt; Frihy et al., 2010; Refaat and Eldeberk, 2016; Ismail, et al., 2012), d)
 108 Gulf of Guinea, West Africa (Lagos in Nigeria; Nwilo et al., 1997; Olaniyan and Afiesimama, 2003) and e) Majuro in
 109 Marshall Pacific Islands (Hoeke et al., 2013). Our TWL minus wave runup estimate (dashed black) is compared with GESLA
 110 tidal gauges (thin black). Total sea level at the coast, including wave runup (thick black) is compared to coastal elevation

111 reported in the literature. Overtopping/flooding happen if total sea level is larger than maximum coastal elevation
112 considered for overtopping.

113

114

115 REFERENCES

116 Athanasiou, P., van Dongeren, A., Giardino, A., Vousdoukas, M., Gaytan-Aguilar, S., and Ranasinghe, R.: Global distribution
117 of nearshore slopes with implications for coastal retreat, *Earth Syst. Sci. Data*, 11, 1515–1529,
118 <https://doi.org/10.5194/essd-11-1515-2019>, (2019).

119 Bertin, X., Bruneau, N., Breilh, J.-F., Fortunato, A. B. & Karpytchev, M. Importance of wave age and resonance in storm
120 surges: The case xynthia, bay of biscay. *Ocean. Model.* 42, 16 – 30 (2012).

121 Diaz, H., Almar, R. & Bergsma, E. W. J. On the use of satellite-based digital elevation models to determine coastal
122 topography. *IEEE proceedings IGARSS, Jpn.* (2019).

123 Ford, M., Merrifield, M. & Becker, J. Inundation of a low-lying urban atoll island: Majuro, marshall islands. *Nat. Hazards*
124 91(3), 1273–1297 (2018).

125 Frihy, O., Deabes, E. & El Gindy, A. Wave climate and nearshore processes on the mediterranean. *J. Coast. Res.* 26(1), 103–
126 112 (2010).

127 Fritz, H. M. et al. Hurricane katrina storm surge distribution and field observations on the mississippi barrier islands.
128 *Estuarine, Coast. Shelf Sci.* 74, 12 – 20 (2007).

129 Hoeke, R. et al. Widespread inundation of pacific islands triggered by distant-source wind-waves. *Glob. Planet. Chang.* 108,
130 128–138 (2013).

131 Ismail, N., Iskander, M. & El-Sayed, W. Assessment of coastal flooding at southern mediterranean with global outlook for
132 lowland coastal zones. *Coast. Eng. Proc.* 33(83), 1–13 (2012).

133 Nwilo, P. C. Managing the impacts of storm surges on victoria island, lagos, nigeria. *Destr. Water: Water-Caused Nat.*
134 *Disasters, their Abat. Control.* IAHS Conf. held at Anaheim, California, June 1996 239, 325–330 (1997).

135 Olaniyan, E. & Afiesimama, E. Understanding ocean surges and possible signals over the nigerian coast: a case study of the
136 victoria island bar-beach lagos. <http://iodeweb1.vliz.be/odin/bitstream/1834/420/1/AniolaNigeria.pdf> (accessed April
137 8, 2019) (2003).

138 Refaat, M. & Eldeberky, Y. Assessment of coastal inundation due to sea-level rise along the mediterranean coast of egypt.
139 *Mar. Geod.* 39:3-4, 290–304 (2016).

140 Scussolini, P. et al. Flopros: an evolving global database of flood protection standards. *Nat. Hazards Earth Syst. Sci.* 16,
141 1049–1061, DOI: 10.5194/nhess-16-1049-2016 (2016).

142 Vousdoukas, M. L. V. E. V. M. J. S. J. L. F. L., M.I. Global probabilistic projections of extreme sea levels show intensification
143 of coastal flood hazard. *Nat. Commun.* 9, 2360 (2018).

144 Woodworth, P.L., Hunter, J.R. Marcos, M., Caldwell, P., Menendez, M. and Haigh, I. 2017. Towards a global higher-
145 frequency sea level data set. *Geoscience Data Journal*, 3, 50-59, doi:10.1002/gdj3.42.